Experimental and Predicted Pressure and Heating Distributions for Aeroassist Flight Experiment Vehicle

John R. Micol*
NASA Langley Research Center, Hampton, Virginia 23665

Pressure and laminar heat-transfer rate distributions measured over the forebody of 2.2% scale (3.67-in.-diam) models of the Aeroassist Flight Experiment vehicle in air at Mach 10 are presented for a range of angles of attack of from −10 to 10 deg. Two values of freestream Reynolds number based on model diameter in the symmetry plane of the base were tested, 1.63 and 6.48 × 10^5. Predictions from an inviscid flowfield code referred to as HALIS (High ALpha Inviscid Solution) and a Navier-Stokes solver referred to as LAURA (Langley Aerothermodynamic Upwind Relaxation Algorithm) were in good agreement with pressure measurements. Heat transfer rates predicted with the LAURA code were generally in good agreement with measurements over the cone and skirt sections but tended to underpredict measurements in the stagnation region.

Nomenclature

C_h = heat transfer coefficient, lbm/ft²-s, $= \dot{q}/(h_{aw} - h_w)$, where $h_{aw} = h_{t,2}$
$C_{h,ref}$ = reference heat transfer coefficient, lbm/ft²-s
C_p = pressure coefficient, $= (p - p_\infty)/q_\infty$
$C_{p,ref}$ = reference pressure coefficient
h = enthalpy, Btu/lbm
L = model diameter in symmetry plane, in. (see Fig. 3)
M = Mach number
p = pressure, psi
q = dynamic pressure, psi
$\dot{q}$ = heat transfer rate, Btu/ft²-s
r = radius, in.
Re = unit Reynolds number, ft^{-1}
s = wetted surface length from geometric stagnation point along instrumentation ray Φ, in.
t = time, s
T = temperature, °R
V = velocity, ft/s
α = angle of attack, deg
γ = ratio of specific heats
ρ = density, lbm/ft³
τ = arc angle, deg (see Fig. 1)
Φ = ray angle from geometric stagnation point, deg (see Fig. 3)

Subscripts
aw = adiabatic wall
b = base
$t,1$ = reservoir conditions
$t,2$ = stagnation conditions behind normal shock
w = model surface; wall surface
2 = static conditions behind normal shock
∞ = freestream static conditions

Presented as Paper 89-1731 at the AIAA 24th Thermophysics Conference, Buffalo, NY, June 12–14, 1989; received Nov. 10, 1989; revision received July 20, 1990; accepted for publication Aug. 3, 1990.

*Aerospace Engineer, Experimental Hypersonics Branch, Space System Division. Member AIAA.

Introduction

THE task of transferring cargo from low to high (e.g., geosynchronous) Earth orbit will be performed by vehicles formerly referred to as orbital transfer vehicles (OTVs) and more recently referred to as space transfer vehicles (STVs). Upon return of the vehicle from high Earth orbit, its velocity must be reduced greatly to achieve capture in low Earth orbit. This decrease in velocity can be achieved either by use of retrorockets or by guiding the vehicle through a portion of the Earth's atmosphere and allowing aerodynamic drag forces to act on the vehicle (i.e., aeroassist). A number of studies have indicated that lower propellant loads are required, and therefore payloads are increased, for the aeroassist method.[1,2] Vehicles using the aeroassist method, generally referred to as aeroassisted orbital transfer vehicles (AOTVs), or aeroassisted space transfer vehicles (ASTVs), will require a low lift-to-drag ratio (L/D) and will fly at very high altitudes and velocities throughout the atmospheric portion of the trajectory. Because of the high-altitude, high-velocity trajectory, flight experience is scarce, and ground-based facilities cannot duplicate and, in general, not simulate the flow environment.

Because of the lack of information from either previous flights or ground-based simulation, a precursor experimental ASTV flight has been proposed and is referred to as the Aeroassist Flight Experiment (AFE). (See Ref. 3 for a comprehensive discussion of the rationale for this flight experiment.) The proposed AFE vehicle is basically a blunted, 60-deg half-angle, raked-off elliptic cone with a rounded corner at the base and has an L/D of about 0.3. The vehicle will be transported by the Space Shuttle Orbiter and placed into low Earth orbit. An onboard rocket motor will then propel the vehicle into the atmosphere to simulate the velocity and trajectory of a return mission from geosynchronous orbit. Onboard instrumentation will measure and record the aerodynamic characteristics and aerothermodynamic environment of this entry condition. The data will be used to validate computational fluid dynamic (CFD) computer codes, engineering methods, and ground-to-flight extrapolations for use in future ASTV designs. The aerodynamic/aerothermodynamic design of the AFE vehicle, however, must rely on experimental wind-tunnel data and predictions from CFD codes that need to be calibrated with the best available data from ground-based facilities.

Recently, a set of high-fidelity AFE models was designed, constructed, and tested at the Langley Research Center to obtain aerodynamic and aerothermodynamic data over a wide range of conditions.[4,5] In addition, CFD codes were applied to the proposed configuration and provided predictions of

forces and moments, pressures, and heating.[6-8] The purpose of this paper is to present pressure distributions and heat transfer rates measured over the AFE configuration in the Langley 31-Inch Mach 10 Tunnel and compare predictions with an inviscid flowfield code referred to as HALIS (High ALpha Inviscid Solution[6]) and a Navier-Stokes code referred to as LAURA (Langley Aerothermodynamic Upwind Relaxation Algorithm[8]) to the experimental data. These experimental and computational results are expected to be of great interest to the designers of the AFE aeroshell and to the principal investigators of the various onboard experiments.

Experimental Method

Facility

The Langley 31-Inch Mach 10 Tunnel, formerly known as the Langley Continuous-Flow Hypersonic Tunnel,[9] is a blowdown facility having a run time of approximately 60 s. The facility uses a water-cooled, three-dimensional contoured nozzle to generate a nominal Mach number of 10 at the 31-in. square test section. Dry air is used as the test gas and is heated to a maximum reservoir stagnation temperature of 1900°R. The maximum reservoir pressure is 1450 psi. The tunnel is equipped with a sidewall-mounted model injection/retraction system. Models are sheltered in the injection chamber on the side of the tunnel until the tunnel flow is started. After establishing Mach 10 flow at the test section, models are injected into the highly uniform stream within 0.5 s.

Models

Pressure and heat transfer distributions were measured on 0.022-scale (3.67-in.-diam) models of the AFE vehicle configuration (Fig. 1). The AFE vehicle shape is a 60-deg elliptic cone raked off at a 73-deg angle. The cone is blunted with an ellipsoid nose (ellipticity equal to 2.0), which is tangent to the cone at all points of their intersection. A skirt having an arc radius equal to one-tenth of the diameter of the rake plane and an arclength corresponding to 60 deg has been attached to the rake plane. The circular arc is tangent to the cone in all meridional planes. A geometrical description of this configuration is presented in Ref. 10.

The 3.67-diam AFE pressure model (Fig. 2) was machined from stainless steel and fabricated with 67 pressure orifices (0.040 in. diameter) distributed along seven rays emanating from the geometric stagnation point (Fig. 3); two base pressure orifices (0.60 in. diameter) were located along the 0- and 180-deg rays on the base (r/r_b = 0.782). The 3.67-in.-diam AFE heat transfer model (Fig. 4) was fabricated from a machinable glass-ceramic.[11] Instrumentation for the heat transfer model was distributed along the same seven rays (Figs. 3 and 4) to match the orifice distribution on the pressure model.

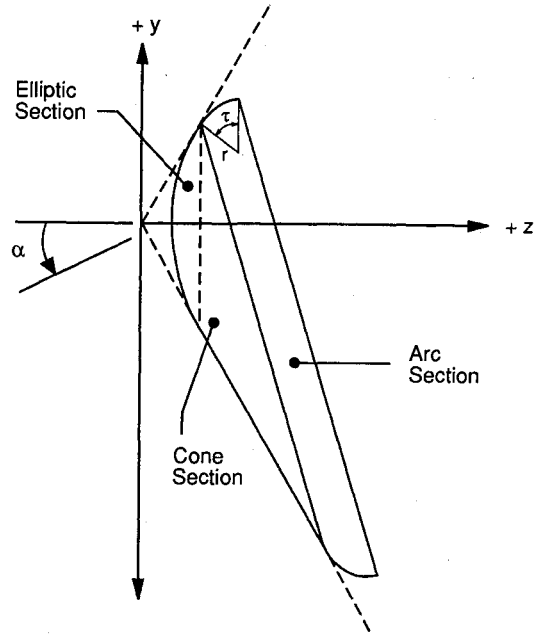

Fig. 1 Sketch of AFE model (r = 0.3344 in.; τ = 60 deg).

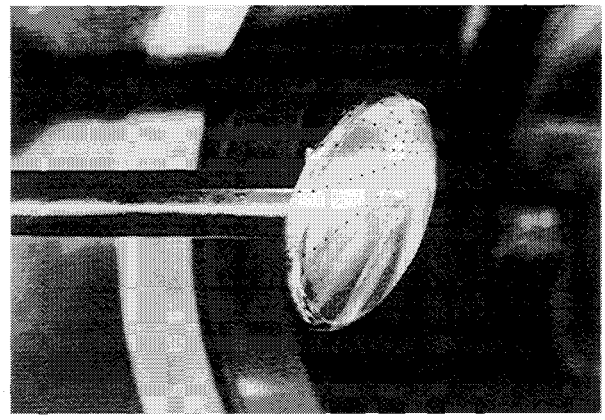

Fig. 2 Photograph of AFE pressure model.

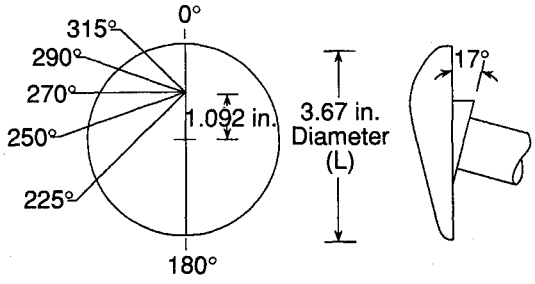

Fig. 3 Location of instrumented rays for AFE pressure and heat transfer models.

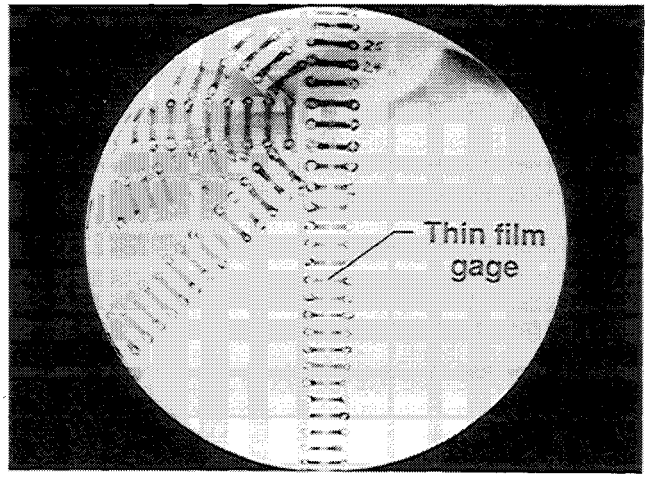

Fig. 4 Photograph of AFE heat transfer model (layout of instrumented rays).

For this CFD code calibration study, both models were cut on a numerical milling machine from a tape generated with the geometry program described in Ref. 10. Since this program was also used to generate the geometry in the HALIS code (to be discussed subsequently), differences between the experimental and computational model were minimal (i.e., within a machining tolerance of ±0.003 in.).

Test Conditions

For the present study, pitot pressure could not be measured conveniently when the model was positioned in the test sec-

tion; hence, test-section flow conditions were obtained using measured reservoir pressures and temperatures and a recent unpublished calibration of the facility. Nominal reservoir stagnation and corresponding freestream flow conditions for the present study are presented in Table 1.

Both the pressure and heat transfer models were tested over an angle-of-attack range of from −10 to 10 deg in 5-deg increments for each flow condition; the yaw angle was zero for all tests. Angle of attack is defined as the incidence between the flow direction and the axis of the 60-deg elliptic cone (Fig. 1). The α range for the flight vehicle is −5 to 5 deg. The value of L used to determine $Re_{\infty,L}$ is 3.67 in.

Instrumentation

Model surface pressures were measured using an electronically scanned pressure (ESP) system. Each scanner consisted of 32 silicon piezoresistive pressure transducers mounted to a common substrate. For this study, two scanners were used, which provided 64 pressure transducers. Details and application of the ESP system in the Hypersonic Facilities Complex at Langley are discussed in Refs. 12 and 13. The sampling rate for the ESP system was 8 samples/s for each of the 64 channels, and the pressure range for the transducers was 0–5 psi.

Thin-film resistance heat transfer gauges were used to measure surface temperature-time histories from which heat transfer rates were inferred. The technology of the thin-film gauges remains unchanged from that developed for the Langley Expansion Tube.[14,15] Unlike previous studies in which heat transfer models were fabricated from steel and then slotted to accept machinable glass-ceramic substrates, the present model is unique because it was machined entirely from the ceramic. By making the model in this manner, the uncertainty associated with the discontinuities in thermal conductivity for a stainless steel model with inserts is eliminated.[16] Seventy-three palladium gauges (0.04 × 0.05 in.), each approximately 1000 Å thick, were deposited on the polished surface of the model. The model thickness was sized to provide a maximum run time of 1.5 s; i.e., the substrate (which is the model) essentially behaves as a semi-infinite slab for 1.5 s over most of the forebody. An aluminum oxide overlayer, approximately 5000 Å thick, was deposited over the sensing element as a means of increasing gauge durability. Detailed discussions of gauge construction, circuitry, calibration procedures, and the data acquisition system are discussed in Refs. 13 and 15.

Data Reduction and Uncertainty

The 60-s run time of the 31-Inch Mach 10 Tunnel allowed pressure measurements to be made at several angles of attack during a run. Of particular concern in pressure measurements is the lag time required for the pressure measurement system to measure, transmit, and record accurately the value of pressure at the model surface for a particular set of test conditions. In the present study, pressure tube lengths from the orifices to the measuring device were on the order of 5 ft. The pressure modules were located within an insulated box positioned on the injection carriage assembly. For this arrangement, typical settling times for surface pressures measured on the windward face were within 2 s from the moment of insertion into the flow and base pressures required approximately 5 s to reach steady-state values. As the model angle of attack was varied, pressure settling times were on the order of 0.5 s after the α setting was reached. Comparisons of data repeatability for identical runs at $\alpha = 0$ deg and a Reynolds number of 6.48 × 10^5 indicated that measured pressures for the windward centerline agreed to within ±0.5%. In a previous study,[5] variable-capacitance diaphragm transducers were used selectively to measure pressures simultaneously with the pressure scanner system transducers. Measurements between the two systems generally agreed to within 0.5%; the maximum difference observed was 1.5%. For the present study, the uncertainty of the pressure measurements presented is believed to be less than ±2.0%.

Table 1 Nominal reservoir and freestream flow conditions

$p_{t,1}$, psi	$T_{t,1}$, °R	p_∞, psi	T_∞, °R	M_∞	$Re_{\infty,L} \times 10^{-5}$
348.6	1835	0.00941	95.89	9.74	1.63
1449.0	1822	0.03239	89.99	10.05	6.48

The numerical method used to compute values of heat transfer rate $\dot{q}$ from the output of the thin-film resistance gauges is discussed in Refs. 15 and 17. A more accurate determination of the thermal properties of the glass-ceramic material[18] was used to reduce the data for the present study than was presented in Ref. 15. Sample time histories for gauges along the windward centerline revealed the heat transfer coefficient C_h was essentially constant (i.e., within ±2%) over the time interval from 0.5 to 1.7 s; i.e., the substrate behaved one-dimensionally. For gauges on the skirt, C_h was observed to increase with time, indicating that gauges in this region of small surface radius do not behave one-dimensionally, as expected. Second-order, least-square curve fits were applied to time histories of $\dot{q}$ for $0.5 < t < 1.7$ s, and values of $\dot{q}$ (or C_h) presented herein were obtained from these curve fits and correspond to $t = 1.1$ s unless otherwise noted. (For example, $\dot{q}$ inferred from gauges on the skirt region corresponds to $t = 0.5$ s.) Run-to-run repeatability for the thin-film heat transfer technique for $\alpha = 0$ deg and a Reynolds number of 1.63 × 10^5 was within ±1.1%. For the $Re_{\infty,L} = 6.48 \times 10^5$ case, a maximum run-to-run variation of ±3.5% was noted. Probable sources of error for thin-film resistance gauges are discussed in Refs. 15 and 16; based on these discussions and the present run-to-run variations, the heat transfer rates presented herein are believed accurate to within ±8%.

Prediction Methods

HALIS Code

One of the methods used to predict surface pressure distributions is the HALIS code.[6,7,19,20] HALIS, a time-asymptotic method that solves the time-dependent, three-dimensional, compressible Euler equations, was developed for the CDC Cyber 205 vector processing computer.[19] The use of vector processing allows HALIS to compute the flowfield over complex three-dimensional bodies with large embedded subsonic regions in 75 min. Gridding used in the HALIS code and the computational geometry are discussed in Refs. 6 and 7. The basic inputs to HALIS, in terms of flow conditions, were nominal values of M_∞ and γ_∞ for ideal air.

LAURA Code

Surface pressure distributions and heating rates for the AFE geometry were calculated using LAURA. This code has been improved continually over the past few years and is described in detail in Refs. 8 and 21–24. (The latest version of the code is described in Ref. 24.) LAURA is a finite-volume–based algorithm that employs a point-implicit relaxation procedure for obtaining the numerical solution to the governing equations (Navier-Stokes) for three-dimensional, viscous, hypersonic flows, including chemical and thermal nonequilibrium when appropriate. (It should be noted that LAURA was exercised to provide wake flow characteristics as well as forebody flow characteristics, and comparisons to experimental data are presented in Ref. 25.) A multidomain grid is used in the LAURA calculations to provide better resolution of the free shear layer coming off the forebody shoulder. LAURA was exercised for a perfect gas with the basic inputs, in terms of flow conditions, being V_∞, T_∞, and ρ_∞.

Results and Discussion

Effect of Angle of Attack

Measured pressure distributions for the AFE configuration are presented in Fig. 5 for a range of angles of attack and a

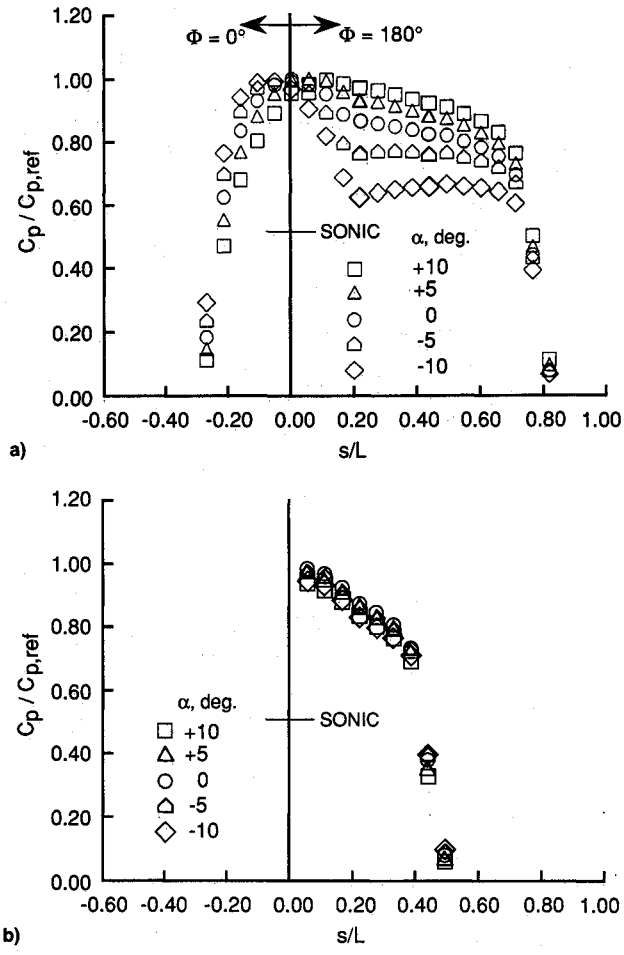

Fig. 5 Effect of angle of attack on pressure distributions; Mach = 10; air; $Re_{\infty,L}$ = 1.63 × 10⁵. a) Φ = 0 and 180 deg. b) Φ = 270 deg.

Reynolds number of 1.63 × 10⁵. The data are presented for the Φ = 0-, 180-, and 270-deg rays. The variation of the pressure coefficient ratio, $C_p/C_{p,\text{ref}}$, with wetted surface length, s/L, for the symmetry plane (Φ = 0 and 180 deg) is presented in Fig. 5a. Along the Φ = 0-deg ray, the pressures are well behaved and increase with decreasing α. A slight overexpansion of the flow from the ellipsoid nose to the conical surface is observed along the Φ = 180-deg ray for $\alpha = -10$ deg but is not observed at $\alpha \geq -5$ deg. This overexpansion is due to the influence of the cone section on the expansion over the nose. [Reference 5 indicates that this overexpansion becomes significantly more prominent with decreasing γ (ratio of specific heats).] Also noted for the symmetry plane is the characteristic movement of the region of maximum pressure with varying angle of attack. As α is decreased from zero, the stagnation region is relatively well defined and moves farther up and around the elliptical nose along the Φ = 0-deg ray, as expected. However, as α is increased from zero, the stagnation region takes the appearance of a relatively large pressure area centered around the juncture of the elliptical nose and conical surface (s/L = 0.22); i.e., at high α, the pressure distribution is similar to the distribution for a flat-faced cylinder with rounded corners. The 20-deg variation in α presented in Fig. 5 produces a change in the pressure ratio of 30–50% on the cone section. In addition, the flow over the nose and cone section is subsonic ($M < 1$) for all values of α. (Note that if the flow within the shock layer expands isentropically from the stagnation region, it will become supersonic when $C_p/C_{p,\text{ref}} < 0.5175$.) Trends for the Φ = 225- and 250-deg rays (not shown) were similar to those for the Φ = 180-deg ray. For the Φ = 270-deg ray (Fig. 5b), which is orthogonal to the symmetry plane, values of $C_p/C_{p,\text{ref}}$ are essentially independent (to within ±2.7% for $s/L < 0.4$) of changes in angle of attack. For the Φ = 290- and 315-deg rays (not shown), $C_p/C_{p,\text{ref}}$ was once again dependent on α and exhibited similar trends to those observed along the Φ = 0-deg ray.

Measured heating distributions for the AFE are presented in Fig. 6 for the same range of angles of attack and a Reynolds number of 1.63 × 10⁵. The data are presented for all rays. The variation of heat transfer coefficient ratio, $C_h/C_{h,\text{ref}}$, with wetted surface length, s/L, for the symmetry plane (Φ = 0 and 180 deg) is presented in Fig. 6a. For the Φ = 0-deg ray, a movement of the stagnation region farther up and around the elliptical nose is observed with decreasing α. In addition, the magnitude of the heating over the elliptical nose increases with decreasing α. The reason for this increase is due to changes

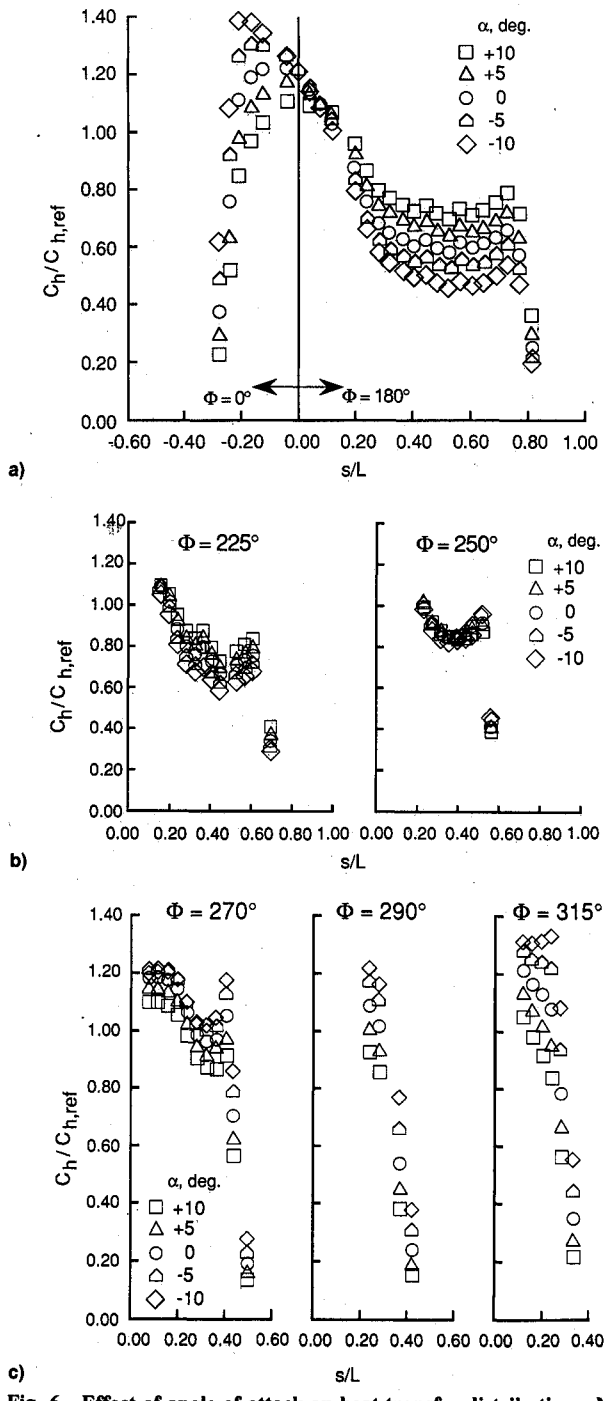

Fig. 6 Effect of angle of attack on heat transfer distributions; Mach = 10; air; $Re_{\infty,L}$ = 1.63 × 10⁵. a) Φ = 0- and 180-deg rays. b) Φ = 225- and 250-deg rays. c) Φ = 270-, 290-, and 315-deg rays.

in the effective nose radius; i.e., as α is decreased, the effective radius of curvature of the nose, as perceived by the stagnation streamline, varies. With decreasing α, the stagnation region moves to the nose-skirt junction ($s/L = -0.2$). For $\alpha = 0$ deg, the geometric stagnation point of the model (0,0) and the center of the measured region of maximum heating do not coincide, since the center is displaced slightly farther up on the nose along the $\Phi = 0$-deg ray. Along the $\Phi = 180$-deg ray, the heating decreases away from the stagnation region, as expected, rapidly at first but levels out over the cone section ($0.22 \leq s/L \leq 0.61$). As the skirt is approached, the heating increases and reaches a peak near $s/L = 0.73$. This increase in heating in the vicinity of the skirt is the result of the rapid acceleration of the flow in this region. Along the $\Phi = 180$-deg ray for $s/L > 0.2$, heating rates over the cone and skirt increase with increasing α. The 20-deg variation in α (corresponding to the same α variation for the pressure data) produces a heating rate change of approximately 50% over the cone section and a 25% change over the ellipsoidal nose section.

For the $\Phi = 225$-deg ray (Fig. 6b), the measured heating rates decrease rapidly over the cone section for $0.20 \leq s/L \leq 0.41$ and then increase as the flow approaches the skirt as a result of flow acceleration to the corner. Heating rates decrease with decreasing α for $s/L \geq 0.20$. For the $\Phi = 250$-deg ray, $C_h/C_{h,\text{ref}}$ is essentially independent (to within $\pm 2.7\%$ for $s/L < 0.5$) of changes in angle of attack (-10 deg $\leq \alpha \leq 10$ deg). Again, the trend of the heating data is to decrease away from the stagnation region and then increase in the direction of the skirt.

For the $\Phi = 270$-deg ray (Fig. 6c), the heating rate is again dependent on α; however, a reversal of the trends noted for $\Phi = 180$ and 225 deg has occurred. That is, for increasing angle of attack, there is a decrease in heating rate. $C_h/C_{h,\text{ref}}$ is nearly constant for $s/L < 0.2$ and approaches a value of about 1.2 with decreasing α. For $s/L > 0.2$, the familiar cusp trend in the heating data is observed. One interesting observation is that the peak heating at the cone-skirt junction ($s/L = 0.41$) approaches the same value of the heating rate measured near the geometric stagnation point for $\alpha \leq -5$ deg. For the $\Phi = 290$- and 315-deg rays (Fig. 6c), the heat transfer rate increases with decreasing α. This increase in $C_h/C_{h,\text{ref}}$ is consistent with the movement of the stagnation region farther up onto the ellipsoid nose as α becomes more negative. In addition, for the $\Phi = 315$-deg ray, the heat transfer rate varies linearly for $0 < s/L < 0.28$. The slopes of the linear fits to the data in this region decrease with decreasing α and finally approach a constant value of $C_h/C_{h,\text{ref}}$ for $\alpha = -10$ deg.

Reynolds Number Effects

Pressure and heat transfer distributions for $Re_{\infty,L} = 1.63 \times 10^5$ and 6.48×10^5 are shown in Figs. 7 and 8, respectively, for $\alpha = 0$ deg and $\Phi = 0$ and 180 deg. As expected for the blunt AFE configuration, there is a negligible effect on the nondimensionalized forebody pressure ($C_p/C_{p,\text{ref}}$) distributions for this factor of 4 variation in Reynolds number; although not shown, this was the case for all angles of attack. There is, however, a measurable increase in the nondimensionalized heat-transfer rate ($C_h/C_{h,\text{ref}}$) distributions with decreasing Reynolds number. Previous unpublished results of measured stagnation-point heat transfer rate to a 4-in.-diam sphere at the same two values of $Re_{\infty,L}$ in the same facility and using the same data reduction procedures revealed similar variations of $C_h/C_{h,\text{ref}}$ with Reynolds number. Thus, the increase in heating with Reynolds number observed in Fig. 8 may be due, in part, to the reference value of the heat transfer coefficient. When measured values of C_h for the AFE model are normalized by measured values for the 4-in.-diam sphere, data for the two values of Reynolds number agree to within the experimental uncertainty (8%), thereby precluding a conclusion on the effect of Reynolds number on heating.

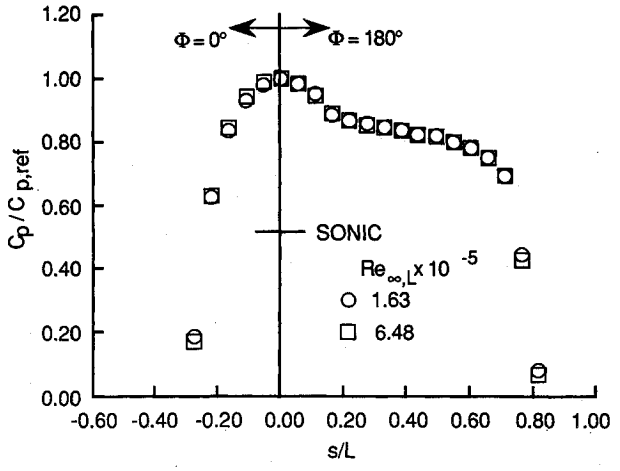

Fig. 7 Effect of Reynolds number on measured pressure distributions; Mach = 10; air; $\alpha = 0$ deg.

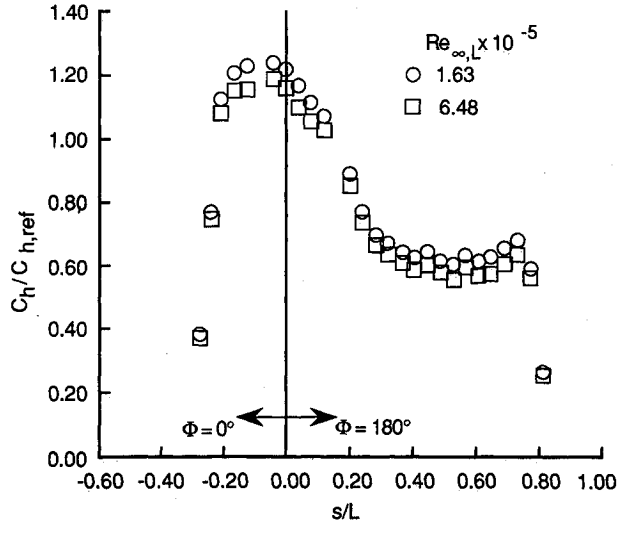

Fig. 8 Effect of Reynolds number on measured heat transfer distributions; Mach = 10; air; $\alpha = 0$ deg.

Comparisons with Prediction

Comparisons of measured and predicted pressure distributions in the plane of symmetry at a Reynolds number of 1.63×10^5 are presented for $\alpha = 0$, 5, and -5 deg in Fig. 9. For all angles of attack, both the HALIS and LAURA codes predict the measured pressure distributions over the nose and cone section with good (within 3–4%) agreement. One possible explanation for the slight overprediction in pressure over the cone section ($\Phi = 180$ deg) by HALIS and differences between HALIS and LAURA may be the grid resolution in this region. (A finer grid was used in the LAURA calculations and is described in Ref. 24.) The modified Newtonian theory and the measured data are in good agreement over the elliptical nose, but in poor agreement over the cone section ($0.2 < s/L < 0.7$).

Comparisons of measured and predicted nondimensionalized heat transfer distributions in the plane of symmetry at a Reynolds number of 1.63×10^5 are presented in Fig. 10 for $\alpha = 0$, 5, and -5 deg. The computational data have been normalized by the same reference heating value as the measured heating rates. For $\alpha = 0$ deg (Fig. 10a), the LAURA code predicts the measured heating rates over the cone section ($0.22 \leq s/L \leq 0.70$) to within 8–10%; however, in the stagnation region, LAURA tends to underpredict the measurements by up to 15%. As discussed in Ref. 24, the larger differences between measurement and prediction in the stagnation region are believed to be due to truncation errors associated with the singularity at the geometric stagnation

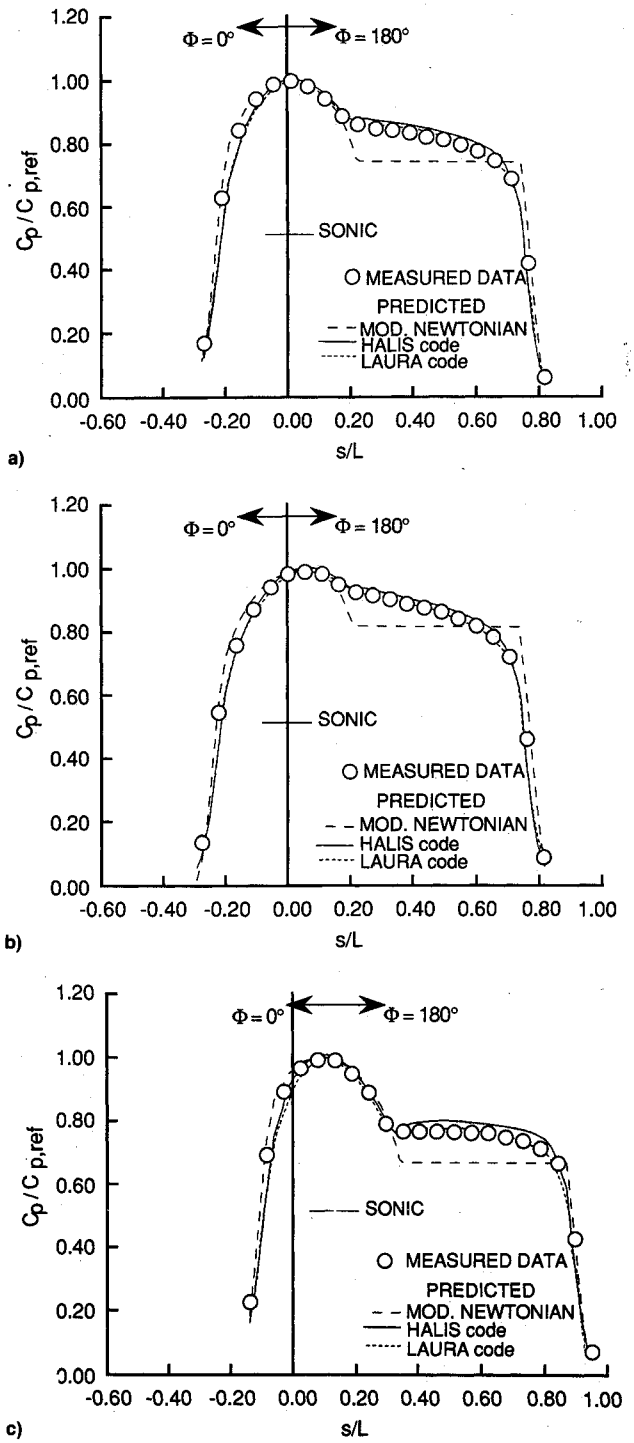

Fig. 9 Comparison of measured and predicted pressure distributions; Mach = 10; $Re_{\infty,L}$ = 1.63 × 10⁵. a) α = 0 deg. b) α = 5 deg. c) α = −5 deg.

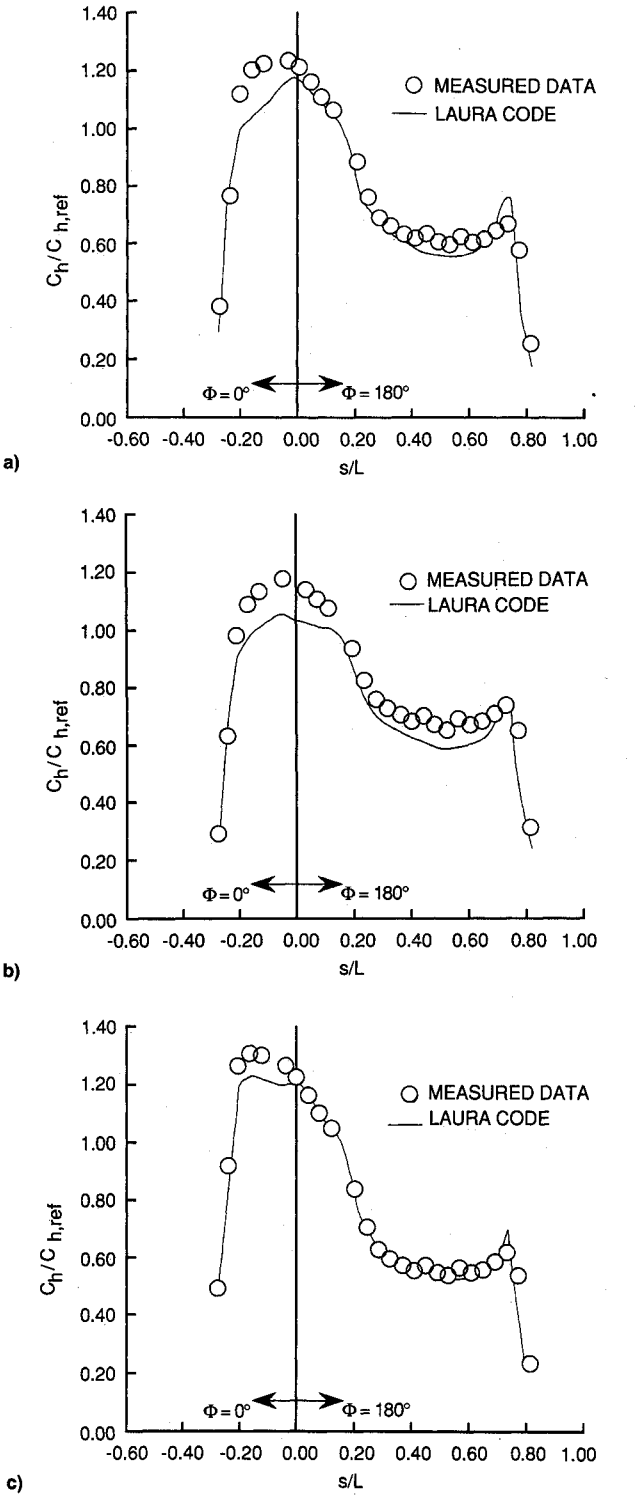

Fig. 10 Comparison of measured and predicted heat transfer distributions in air at Mach 10; $Re_{\infty,L}$ = 1.63 × 10⁵. a) α = 0 deg. b) α = 5 deg. c) α −5 deg.

point. For α = 5 deg (Fig. 10b), LAURA predictions are in good agreement (within experimental uncertainty of ±8%) with measurement over the cone and skirt, but poorer agreement in the stagnation region. The LAURA code generally shows good agreement with the measured distribution for α = −5 deg (Fig. 10c). The stagnation region heating at the ellipsoid nose-skirt corner (s/L = − 0.2) and the enhanced heating at the corner of the cone and skirt junction (s/L = 0.73) are modeled well by LAURA.

Summary of Results

Pressure and laminar heat-transfer rate distributions were measured over the forebody of 2.2%-scale (3.67-in.-diam) models of the Aeroassist Flight Experiment vehicle in air at Mach 10. Predictions from an inviscid flowfield code, HALIS (High ALpha Inviscid Solution), and a Navier-Stokes solver, LAURA (Langley Aerothermodynamic Upwind Relaxation Algorithm), were compared with the measured values in the plane of symmetry.

The effect of Reynolds number on forebody pressure distributions was negligible for the limited range of this study. As the angle of attack decreased from 10 to −10 deg, the pressure distribution showed a slight overexpansion of the flow from the ellipsoid nose onto the cone at the lowest angle. Pressure distributions predicted with HALIS and LAURA were generally in good agreement with measurements, whereas

those predicted with modified Newtonian theory were in good agreement over the nose, but in poor agreement over the cone section.

The effect of Reynolds number on heat transfer distributions was quite small (i.e., generally within the experimental uncertainty). Varying the angle of attack over a range of from 10 to −10 deg produced a movement of the stagnation region up and around the nose and onto the skirt. In addition, the magnitude of the stagnation region heat transfer rate increased by 25% with decreasing α, corresponding to a smaller effective local radius. Heat transfer rates predicted with the LAURA code were generally in good agreement with measurement over the cone and skirt sections, but tended to underpredict measurement in the stagnation region. Agreement between measured and predicted heat transfer distributions improved in the stagnation region with decreasing angle of attack.

Acknowledgments

This research reported herein is a portion of work being done in partial fulfillment of the requirements for the degree of Master of Science from George Washington University. The author wishes to acknowledge the contributions of K. J. Weilmuenster and Peter A. Gnoffo of the NASA Langley Research Center's Aerothermodynamics Branch, Space Systems Division, who provided the predictions presented herein.

References

[1]Walberg, G. D., "A Review of Aeroassisted Orbit Transfer," AIAA Paper 82-1378, Aug. 1982.

[2]Roberts, B. B., "System Analysis and Technology Development for the NASA Orbit Transfer Vehicle," AIAA Paper 85-0965, June 1985.

[3]Jones, J. J., "The Rationale for an Aeroassist Flight Experiment," AIAA Paper 87-1588, June 1987.

[4]Wells, W. L., "Wind Tunnel Preflight Test Program for Aeroassist Flight Experiment," AIAA Paper 87-2367, Aug. 1987.

[5]Micol, J. R., "Simulation of Real-Gas Effects on Pressure Distributions for a Proposed Aeroassist Flight Experiment Vehicle and Comparison to Prediction," AIAA Paper 87-2368, Aug. 1987.

[6]Weilmuenster, K. J., and Hamilton, H. H., II, "A Comparison of Computed and Measured Aerodynamic Characteristics of a Proposed Aeroassist Flight Experiment Configuration," AIAA Paper 86-1366, June 1986.

[7]Hamilton, H. H., II, and Weilmuenster, K. J., "Calculation of Convective Heating on Proposed Aeroassist Flight Experiment Vehicle," AIAA Paper 86-1308, June 1986.

[8]Gnoffo, P. A., and McCandless, R. S., "Enhancements to Program LAURA for Computation of Three-Dimensional Hypersonic Flow," AIAA Paper 87-0280, Jan. 1987.

[9]Miller, C. G., III, "Measured Pressure Distributions, Aerodynamic Coefficients, and Shock Shapes on Blunt Bodies at Incidence in Hypersonic Air and CF_4," NASA TM 84489, 1982.

[10]Cheatwood, F. M., DeJarnette, F. R., and Hamilton, H. H., II, "Geometrical Description for a Proposed Aeroassist Flight Experiment Vehicle," NASA TM 87714, July 1986.

[11]Grossman, D. G., "Machining a Machinable Glass-Ceramic," *Vacuum*, Publishing & Advertising Offices, Pergamon Press, Maxwell House, Fairview Park, Elmsford, N.Y. 10523, Vol. 28, No. 2, 1978, pp. 55–61.

[12]*Model 780BIT Pressure Measurement System Users Manual*, 1st ed., Sept. 1983.

[13]Miller, C. G., and Smith, F. M., "Langley Hypersonic Facilities Complex-Description and Application," AIAA Paper 86-0741-CP, March 1986.

[14]Miller, C. G., III, Micol, J. R., and Gnoffo, P. A., "Laminar Heat-Transfer Distributions on Biconics at Incidence in Hypersonic-Hypervelocity Flows," NASA TP 2213, 1984.

[15]Miller, C. G., III, "Comparison of Thin-Film Resistance Heat-Transfer Gages with Thin-Skin Transient Calorimeter Gages in Conventional-Hypersonic Wind Tunnels," NASA TM 83197, 1981.

[16]Schultz, D. L., and Jones, T. V., "Heat-Transfer Measurements in Short-Duration Hypersonic Facilities," Printed by Technical Editing and Reproduction Ltd., Harford House, 7-9 Charlotte St., London, W1P 1HD, AGARD-AG-165, Feb. 1973.

[17]Cook, W. J., and Felderman, E. J., "Reduction of Data from Thin-Film Heat Transfer Gages: A Concise Numerical Technique," *AIAA Journal*, Vol. 4, No. 3, 1966, pp. 561–562.

[18]Miller, C. G., III, "Experimental and Predicted Heating Distributions for Biconics at Incidence in Air at Mach 10," NASA TP 2334, 1984.

[19]Weilmuenster, K. J., and Hamilton, H. H., II, "Calculations of Inviscid Flow Over Shuttle-like Vehicles at High Angles of Attack and Comparisons with Experimental Data," NASA TP 2103, 1983.

[20]Micol, J. R., and Weilmuenster, K. J., "Experimental Aerodynamic Coefficients on a Shuttle-like Vehicle at Mach 6 and 10 and Comparison to Prediction," AIAA Paper 85-1796, Aug. 1985.

[21]Gnoffo, P. A., "Application of Program LAURA to Three-Dimensional AOTV Flowfields," AIAA Paper 86-0565, Jan. 1986.

[22]Gnoffo, P. A., and McCandless, R. S., "Three-Dimensional AOTV Flowfields in Chemical Nonequilibrium," AIAA Paper 86-0230, Jan. 1986.

[23]Gnoffo, P. A., and Greene, F. A., "A Computational Study of the Flowfield Surrounding the Aeroassist Flight Experiment Vehicle," AIAA Paper 87-1575, June 1987.

[24]Gnoffo, P. A., "A Code Calibration Program in Support of the Aeroassist Flight Experiment," AIAA Paper 89-1673, June 1989.

[25]Wells, W. L., "Measured and Predicted Aerodynamic Heating on a Cylinder in Wake of AFE Configuration at Incidence," AIAA Paper 89-2162, July 1989.